



HAL
open science

Thermodynamic analysis of carbon dioxide storage in salt caverns to improve the Power-to-Gas process

A. Soubeyran, Ahmed Rouabhi, C. Coquelet

► To cite this version:

A. Soubeyran, Ahmed Rouabhi, C. Coquelet. Thermodynamic analysis of carbon dioxide storage in salt caverns to improve the Power-to-Gas process. *Applied Energy*, 2019, 242, pp.1090-1107. 10.1016/j.apenergy.2019.03.102 . hal-02080773

HAL Id: hal-02080773

<https://minesparis-psl.hal.science/hal-02080773>

Submitted on 22 Oct 2021

HAL is a multi-disciplinary open access archive for the deposit and dissemination of scientific research documents, whether they are published or not. The documents may come from teaching and research institutions in France or abroad, or from public or private research centers.

L'archive ouverte pluridisciplinaire **HAL**, est destinée au dépôt et à la diffusion de documents scientifiques de niveau recherche, publiés ou non, émanant des établissements d'enseignement et de recherche français ou étrangers, des laboratoires publics ou privés.



Distributed under a Creative Commons Attribution - NonCommercial 4.0 International License

Thermodynamic analysis of carbon dioxide storage in salt caverns to improve the Power-to-Gas process

A. Soubeyran^{a,*}, A. Rouabhi^a, C. Coquelet^b

^a*MINES ParisTech, PSL University, Centre de Géosciences, 35 rue St Honoré, 77300 Fontainebleau, France*

^b*MINES ParisTech, PSL University, Centre Thermodynamique des Procédés, 35 rue St Honoré, 77300 Fontainebleau, France*

Abstract

In the current energy transition context, one of the most promising technological solutions to the main complication of the Power-to-Gas process, namely, the supply of carbon dioxide, is to temporarily store carbon dioxide in underground facilities such as salt caverns. However, despite extensive studies on the thermodynamic characteristics of carbon dioxide, the way this gas behaves in a salt cavern has never been described. Such information is essential to enable efficient monitoring of a cavern in accordance with the power demand. This article aims to provide a first analysis of the behavior and specificities of storing carbon dioxide in a salt cavern and subsequently compare the storage behavior of carbon dioxide to that of methane, which is already well known. The comparison is first achieved numerically by simulating the predictive thermodynamic behaviors of both products under different contexts: despite some similarities, no relevant analogy can be easily established between carbon dioxide and methane. The main reasons explaining the different behaviors of the two products are related to their critical point and their capacity of interactions with brine. This last observation is also investigated experimentally by reproducing a cavity at the laboratory scale according to the Pressure-Decay method. The performed experiments show that the phenomenon of mass transfer from dissolution creates a drop in the gas pressure, which is too substantial for carbon dioxide to be neglected. This pressure drop must be accurately characterized to avoid any confusion with pressure drops induced by leakage anomalies in practice.

Keywords: Salt cavern; Carbon dioxide; Underground storage; Thermodynamic behavior;

1. Introduction

In the current energy transition context, the development of new massive energy storage concepts is required to solve the uncontrolled intermittency problem characterizing the energy produced from renewable resources, and make these resources economically viable. Different technologies for energy storage have been proposed, including batteries, flywheels, supercapacitors, or the transformation of the produced energy into a more storable form, including kinetic, potential or chemical energy [1].

Among these solutions, the temporary gas storage is one of the most suitable energy storage solutions at the industrial scale, according to Bauer et al. [2]. Currently, the best-known existing technologies are the CAES (Compressed Air Energy Storage) and PtG (Power to Gas) processes, which are both based on excess electrical energy. The CAES principle consists of using compressed ambient air as a working fluid that is stored in underground reservoirs and expanded in turbines when needed to restore the electrical energy (see Cavallo [3], Succar and Williams [4], or Budt et al. [5]). The aim of the PtG process is to convert excess energy into a chemical energy carrier that is easy to store in reservoirs, as described by Lehner et al. [6], Götz et al. [7], or by ADEME [8]. The most developed process successively produces hydrogen (H_2) and synthetic methane (CH_4) that result from the electrolysis-methanation transformations, which require large quantities of water (H_2O) and carbon dioxide (CO_2). However, a potential weakness of the PtG concept lies in the CO_2 supply: the concentrated sources of CO_2 captured from energy-intensive industries and from biogas could be insufficient to meet the considerable demand. Solutions involving the hybridization of the PtG concept with a chemical looping combustion [9] or an oxy-fuel combustion [10],[11] have been proposed. Some ongoing projects intend to couple the oxy-fuel combustion to the PtG concept to create a closed loop technology called EMO (electrolysis-methanation-oxy-fuel), as described by Bailera et al. [12] or by the ANR [13]. In such a

*Corresponding author

Email address: aurelien.soubeyran@mines-paristech.fr (A. Soubeyran)

process, oxygen (O_2) generated during the electrolysis phase is stored for reuse in the CH_4 oxy-combustion whereas CO_2 resulting from the CH_4 oxy-combustion phase will be used to feed the forthcoming methanation process during the next storage phase. Therefore, the EMO technology requires the possibility to store massively and recover both O_2 and CO_2 , besides CH_4 .

This article must thus be regarded in this context of the development of new energy storage processes because these processes require large-scale reversible storage facilities for the working fluids. Underground reservoirs are probably the optimal solutions to perform this function, as they offer the largest storage capacities (referring to Aneke and Wang [14]) and are expected to be cost-competitive [15]. There are currently two main types of underground reservoirs for fluid storage: porous media reservoirs where the fluid is stored in the pore space, and rock caverns in which the fluid occupies the free space which results from hard rock excavation or rock solution-mining. Although porous media reservoirs have the largest storage capacities, such reservoirs do not function as well as rock caverns for temporary underground storage because the flow rates of injection-withdrawal operations are limited by the rock permeability, which reduces the flexibility of storage in porous media reservoirs and the corresponding adaptability to the needs of renewable energy management. For this reason, the present study focuses on underground storage in rock caverns, which behave such as pressurized vessels, and especially on underground storage in solution-mined caverns, as these caverns offer the best flow rate capacities, as confirmed by Procesi et al. [16]. Underground storage in rock caverns is a mature technique that has been used for several decades for liquid hydrocarbon and natural gas storage and as CAES plants. Nevertheless, recent projects (such as energy storage concepts like those based on EMO) intend to store underground new products, such as CO_2 , whose behaviors in such conditions are not yet known.

To the best of the authors' knowledge, the temporary underground storage ability of CO_2 has never been studied, except in the article by Solomon et al. [17], in which an "intermediate" storage of CO_2 was investigated. Nonpermanent storage of CO_2 has not been considered in the literature, as can be deduced in [18], where this application for CO_2 storage

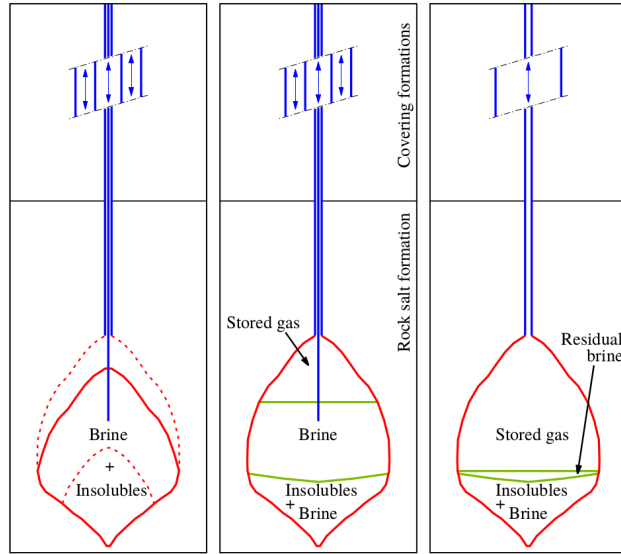


Figure 1: Schematic illustration of the cavern storage facility during the successive phases of leaching, debrining and gas storage operations [24]

is omitted. The underground behavior of CO_2 has been widely studied (examples are given in the works of Bachu [19], De Silva et al. [20], Spycher and Pruess [21], or Ahmadi and Chapoy [22]), but these studies were conducted in a context of long-term sequestration projects and in other geological formations, as explained in [23]. These works can be considered as only a baseline for the present study, as they do not consider some of the thermodynamic aspects inherent to temporary storage. Indeed, in contrast to permanent storage, temporary storage aims to store a product and to recover a large part of the product at any time. This recovery aspect is essential, as any nonrecoverable amount of product corresponds to a loss in the global energy storage process. For this reason, temporary gas storage must be considered not only in terms of capacity, but also of recoverability or maximum transferable mass during injection-withdrawal cycles. The stored product is hence submitted to regular compression-relaxation cycles due to the operations applied on the storage.

The storage history simultaneously includes the succession of performed operations and the process of cavern creation (see Figure 1). The solution-mining process consists of the injection of fresh water, at the depth of the salt formation and the withdrawal of the brine through a well composed of concentric tubes. In addition to the dissolution of the salt, which

is replaced with the brine, the insoluble inclusions embedded inside the rock formation may accumulate at the bottom of the cavern. At the end of the leaching phase, the filling phase begins and the brine is withdrawn from the created cavern, by using a process that depends on the kind of product that will be stored in the cavern. For gas storage, the debrining process consists of the injection of gas through the annular tube, which “pushes” out the maximal amount of brine through the central tube, so that the cavern gets the largest operational volume. The residual thermo-mechanical effects induced during the leaching and debrining steps are likely to impact the thermodynamic conditions of the storage, and consequently, the global behavior of the cavern.

Furthermore, as the debrining operation is not able to withdraw the whole volume of the brine, a residual part of this phase remains at the bottom of the cavern. Consequently, 3 different immiscible phases can coexist within the cavity during its whole life span: the stored fluid (CO_2 in the present case), the brine and the insoluble materials (see Figure 2). These phases interact with each other, exchanging mass and heat, depending on the considered products. The thermodynamic conditions of storage can potentially be affected by this interaction. Therefore, the impact of this interaction on the behavior of the cavern must be well characterized, especially for fluids exhibiting high solubility in brine like CO_2 .

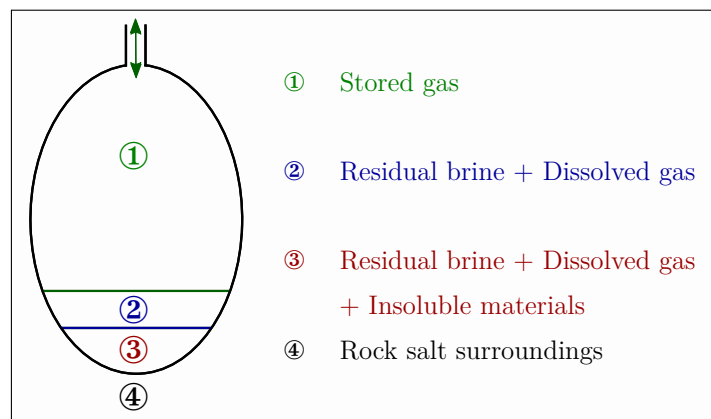


Figure 2: Schematic illustration of the salt cavern storage model [24] adapted for CO_2 storage

Being able to predict the behavior of CO_2 within a cavity is a crucial point for storage

management. From the sizing of the cavity to the elaboration of the most efficient storage scenarios, storage simulations are required to be compared with the evolutions of the observable data in practice and to anticipate any potential risks with respect to the cavity. The monitoring of the cavity is hence strongly dependent on the reliability of the performed storage simulations. If the metered values of the storage during exploitation do not correspond to the simulation results, the storage management will be much more challenging because the operators will not be able to quantify the precise amount of product remaining underground, and may misinterpret the storage data. The goals of this article are to determine whether large volumes of CO_2 can be easily stored within salt caverns, which would make this facility an adapted solution for the development of EMO process at the industrial scale, and to determine which particular phenomena related to CO_2 storage must be studied beforehand and potentially taken into account for the operational phase of the project.

Regarding the complexity of simulating such a system and the complete lack of data to corroborate any result, a preliminary way to model the behavior of CO_2 storage is to assume that the storage of CO_2 behaves similarly to that of other well-known products. For this reason, this study is in the form of a comparison of the thermodynamic behaviors under the same storage conditions of CO_2 and CH_4 which is probably the most well-known product stored in salt caverns. CH_4 is hence considered the reference product in terms of gas storage in salt caverns, due to the large number of studies performed on it (e.g., Bagci and Ozturk [25] or Serbin et al. [26]) and the strong industrial feedback, which is still missing for other products studied in this special context such as compressed air storage [27, 28] and H_2 storage [29, 30]. It is obvious that both gases will respond differently to the same applied loadings due to their different intrinsic features, but the noticed differences can reveal the future points that must be examined before applying CO_2 storage in salt caverns in an energy recovery project such as EMO at an industrial scale. For example, this comparison of the thermodynamic responses of the storage contributes to answering the question of whether the monitoring of CO_2 storage can be adapted from that of CH_4 storage.

The present study must answer the question of whether the CO_2 behaves similarly to CH_4 in a salt cavern environment and how the dissolution ability of CO_2 into the remaining

brine can impact the storage conditions. The paper is organized as follows. Section 2 performs a stepwise comparison of the thermodynamic behaviors of CO₂ and CH₄ under the storage conditions in a salt cavern and presents the main differences between both products, without auguring their importance on the whole storage behavior. Section 3 compares both products experimentally and focuses on the temporal evolution of the mass transfer of CO₂ into the brine, mainly through the characteristic time of this phenomenon.

2. Comparison of the thermodynamic behavior of CO₂ and CH₄ during storage

The thermodynamic behaviors of CO₂ and CH₄ during storage are compared in 3 frameworks: as both products are submitted to idealized transformations (subsection 2.2), as they are stored underground under geostatic conditions (subsection 2.3) and as they are cycled in a salt cavern and interacting with the surroundings (subsection 2.4). The equations adopted to perform these comparisons are first briefly presented in subsection 2.1.

First, the responses of CO₂ and CH₄ to idealized expansions and compressions are studied. The considered idealized transformations are the isenthalpic and the isentropic transformations, which both assume that no heat is exchanged with the surroundings. The temperature evolutions are compared, while the enthalpy h and the entropy s of the products are kept constant respectively. Comparing the behaviors of CH₄ and CO₂ under both isenthalpic and isentropic processes provides a first indication of the thermodynamic response of CO₂ to the different loadings that will be applied to salt cavern storage.

Second, the evolution of the state under which the fluids are stored at geostatic equilibrium is presented. This context must specify how the system tends to evolve, particularly during resting periods, so that the cavern conditions correspond to the surrounding conditions. The equilibrium is defined with the geostatic pressure p_∞ and the geothermal temperature T_∞ , which are linked to the depth z of the storage (assuming here the linear dependence of both p_∞ (in MPa) = 0.022 z and T_∞ (in °C) = 13 + 0.025 z). Attention is given to the evolution of the thermodynamic state of each product with respect to the depth and to the evolution of the solubility of each product into a salt-saturated brine.

Finally, the gases are studied in a real salt cavern storage context. As the CO₂ and CH₄ storage periods are expected to be short compared to the evolution rate of the whole cavity, the global thermodynamic equilibrium is never reached in a salt cavern. The cyclic loading operations tend, on the contrary, to keep the cavern pressure in a predefined range, depending on the characteristics of both the well and the surrounding rock. In the case of gas storage, the cavern pressure remains mostly in the range between $0.2 \times p_\infty$ and $0.8 \times p_\infty$. To compare the behaviors of CO₂ to CH₄, the same storage scenario and assumptions are applied to both. The adopted assumptions for CH₄ storage provide simulation results that have been industrially validated; therefore, using these assumptions to build the model of CO₂ storage is likely to reliably approximate the behavior of this gas. Among the 3 presented comparison contexts, the last framework is obviously the best suited to reproduce the real behavior of CO₂ in salt cavern storage. For this reason, the results of the simulations performed in this context are used to estimate the losses of gas from dissolution into the remaining brine to determine whether further investigations about this phenomenon must be conducted.

2.1. Governing equations

The thermodynamic behavior of the gas is described through the equations of state: among many types of equations submitted in the literature for decades for both CH₄ and CO₂, empirical multiparameter equations of state have been used (Setzmann and Wagner [31] for CH₄, Kunz and Wagner [32] for CO₂), because of their high accuracy at the temperature and pressure ranges found in salt cavern storage. These equations are based on the calculation of a dimensionless form of the Helmholtz free energy, which depends on the temperature and the mass density $\alpha(\rho, T)$. This function, from which all the remaining state functions can be deduced by combining its appropriate derivatives, is split into two parts:

$$\alpha(\rho, T) = \alpha^o(\rho, T) + \alpha^r(\rho/\rho_c, T_c/T) \quad (1)$$

where α^o represents the ideal gas behavior and α^r represents the residual part that corresponds to the deviation from ideality (T_c and ρ_c represent the critical temperature and mass density associated with the considered gas, respectively), which have both been accurately adjusted for CO₂ and CH₄.

Regarding the chemical equilibrium of the gas with the residual brine remaining within the cavity, the Duan-Sun model (elaborated by Duan and Sun for CO₂ [33] and extended to CH₄ by Duan and Mao [34]) has been adopted rather than other existing models (e.g., Spycher and Pruess [21], Akinfiyev and Diamond [35] or Mao et al. [36]) because of the adaptability of the Duan-Sun model for both CO₂ and CH₄ under the thermodynamic conditions of a storage, despite a deviation for salt-saturated brine estimated at approximately 15% according to [37],[38]. The equation of the model is presented as follows:

$$\ln(X_g) = \ln(\phi_g) + \ln(p - p_w) - \mu_g^{l(0)}/RT - 2\lambda_{g-Na}X_{Na} - \zeta_{g-Na-Cl}X_{Na}X_{Cl} \quad (2)$$

where X represents the molality of the chemical species (X is expressed in mol/kg of water, and the subscript of X represents the considered gas or the ions of the brine) in the brine, $\mu_g^{l(0)}(p, T)$ is the standard state of the chemical potential of the gas into the brine phase, $p_w(T)$ is the saturated vapor pressure of pure water, the interaction parameters $\lambda_{g-Na}(p, T)$ and $\zeta_{g-Na-Cl}(p, T)$ are empirical functions, and $\ln(\phi_g)(p, T)$ is the fugacity coefficient determined in this study on the basis of the previously adopted equation of state.

For the thermodynamic problem, the governing equations of the model presented in Rouabhi's model [24] are adopted. In the referenced literature, the authors express the variations in the pressure p and temperature T , which are assumed to be uniform within the whole cavity from the mass and energy balance equations. They can be written as follows:

$$\begin{pmatrix} A_{11} & A_{12} \\ A_{21} & -TA_{11} \end{pmatrix} \begin{pmatrix} \dot{p} \\ \dot{T} \end{pmatrix} = \begin{pmatrix} \dot{\mathcal{W}} \\ \Psi_1 + \Psi_\sigma \end{pmatrix} \quad (3)$$

In this equation system, A_{11} , A_{12} and A_{21} are calculated with the current volume and the corresponding isobaric thermal expansion factor, isothermal compressibility factor and isobaric heat capacity of each phase present within the cavity respectively. The last 3 thermodynamic parameters are calculated from the equation of state related to each phase. $\dot{\mathcal{W}}$, in the mass balance, represents the current cavity volume variation, which is adjusted by the variations in the partial volumes of the different species. Concerning heat transfer, Ψ_σ designates the heat exchanged between the cavern and the surrounding rock salt, whereas

$\Psi_1 = Q^I(H^I - h)$ represents the heat transferred from the in-going matter, where Q^I is the inflow rate, and $H^I(p^I, T^I)$ and $h(p, T)$ are the enthalpies of the in-going matter and the matter contained within the cavern respectively.

To perform the coupling with the surrounding rock salt, which is assumed to be a homogeneous infinite elasto-viscoplastic medium, the calculated pressure and temperature are used as boundary conditions in the thermomechanical problem in the rock salt, whose governing equations can be expressed in spherical coordinates as follows:

$$\begin{aligned}\partial_r \sigma_r + \frac{2}{r}(\sigma_r - \sigma_\theta) &= 0 \\ \partial_r^2 T + \frac{2}{r} \partial_r T &= \frac{\rho C_\sigma}{\Lambda} \dot{T}\end{aligned}\tag{4}$$

where σ_r and σ_θ refer to the radial and tangential components of the stress tensor $\underline{\underline{\sigma}}$ respectively, Λ represents the thermal conductivity of the rock salt surroundings, ρC_σ designates the salt volumetric heat capacity, and $r = r(r_0, t)$ designates the current radial position of the material point, which is initially located at $r_0 \geq a_0$, where a_0 refers to the initial cavity radius. Equation 4 is supplemented by a constitutive law describing the rock salt behavior. As explained by Rouabhi et al. [24] and Labaune and Rouabhi [30], because of the spherical symmetry and assuming infinitesimal elastic strains, the elasto-viscoplastic constitutive law can be written as follows:

$$\begin{aligned}\dot{H}_r &= \frac{1 + \nu}{E} \dot{\sigma}_r - \frac{\nu}{E} \text{tr}(\underline{\underline{\dot{\sigma}}}) + \alpha_\ell \dot{T} + D_r^{vp} \\ \dot{H}_\theta &= \frac{1 + \nu}{E} \dot{\sigma}_\theta - \frac{\nu}{E} \text{tr}(\underline{\underline{\dot{\sigma}}}) + \alpha_\ell \dot{T} + D_\theta^{vp}\end{aligned}\tag{5}$$

where subscripts r and θ designate the radial and tangential components respectively, $H_r = \ln(\partial_{r_0} r)$ and $H_\theta = \ln(r/r_0)$ represent the logarithmic strains in the radial and tangential directions, E is the Young's modulus, ν designates the Poisson's ratio, and α_ℓ represents the linear thermal expansion coefficient. The last term of Equation 5, D^{vp} , refers to the viscoplastic strain rate, whose expanded expression is developed in [24].

Numerical simulations based on this model are performed with the code DEMETHER, developed at MINES ParisTech. This code sequentially solves Equations 3 through 5 at each time step using a Euler implicit scheme in time and one-dimensional finite elements in space.

2.2. Thermodynamic behavior comparison in response to idealized transformations

To perform the comparison, the initial values of the enthalpy h and the entropy s are calculated under the thermodynamic conditions ($p_0 = 10$ MPa, $T_0 = 40^\circ\text{C}$). These conditions are in the range of pressure and temperature experienced during gas storage in salt caverns. The comparison is achieved by varying the pressure between 7 MPa and 20 MPa, which keeps both CO_2 and CH_4 under either a gaseous or supercritical phase. From [Figure 3](#), it can be observed that the global responses of both products are similar, even if the amplitude of the temperature variation due to the loading is lower for CO_2 than for CH_4 . As both products present positive values of $\partial_p T(p, h)$ (Joule-Thomson coefficient) and $\partial_p T(p, s)$, it is deduced that CO_2 and CH_4 tend to cool during adiabatic expansions and inversely heat during compressions. Consequently, it can be expected that CO_2 and CH_4 adopt analogous thermodynamic behaviors when they are submitted to real operations of injection and withdrawal in a salt cavern, which makes the upcoming comparison between them consistent.

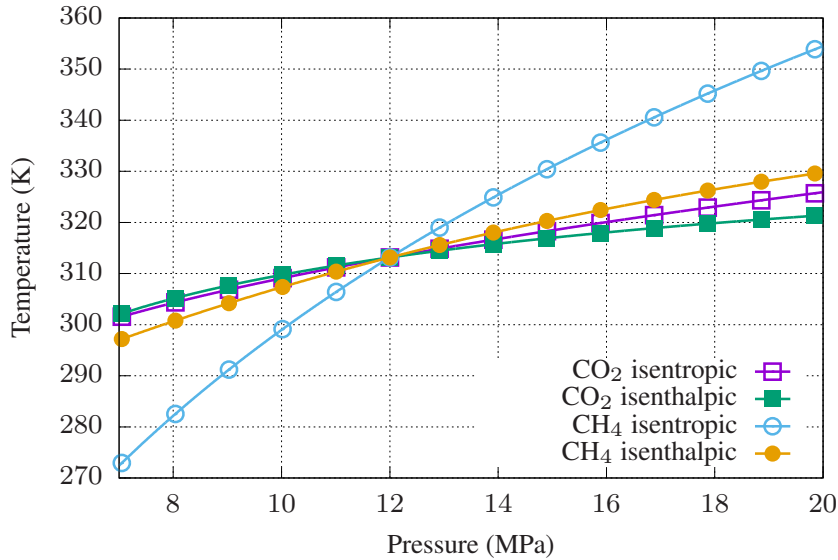


Figure 3: Comparison of the gaseous-supercritical thermal responses of CO_2 and CH_4 to isenthalpic and isentropic transformations at $p_0 = 10$ MPa and $T_0 = 40^\circ\text{C}$

2.3. Thermodynamic behavior comparison under geostatic equilibrium

One of the most suitable thermodynamic variables to recognize the state of a product that is stored underground at equilibrium with the surroundings is the mass density because the discontinuity of the mass density characterizes the separation of the gaseous and liquid phases. The evolution of the mass densities of CO_2 and CH_4 with respect to the storage depth under the underground equilibrium thermodynamic conditions $(p_\infty(z), T_\infty(z))$ is presented in Figure 4. In contrast to CH_4 , which remains in gaseous and supercritical states, CO_2 can also be found under a liquid phase. The discontinuity in the mass density of CO_2 at a 260 m depth (where $p_\infty \approx 5.7$ MPa and $T_\infty \approx 19.5^\circ\text{C}$) reveals a difference in its thermodynamic state: above this limit, both CO_2 and CH_4 are gaseous whereas below the limit, the thermodynamic equilibrium in the cavity can be reached only if CO_2 is liquid. This special case is problematic because the storage management of liquid CO_2 is different than of gaseous CO_2 (as was expected).

Through the evolution of the saturated liquid-vapor density, another limit occurs at a

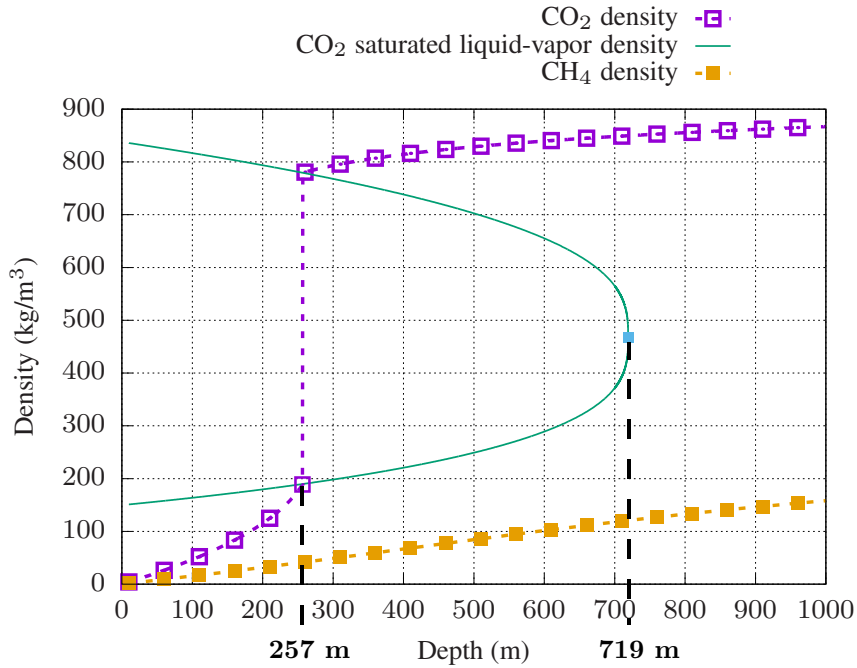


Figure 4: Evolutions of the densities ρ of CO_2 and CH_4 with respect to the depth z under geostatic pressure and geothermal evolution $\rho(p_\infty(z), T_\infty(z))$

depth of 720 m, which separates the liquid from the supercritical phases. At this depth, the geothermal temperature corresponds to the critical temperature of CO₂. At depths greater than 720 m, CO₂ is in equilibrium with the surroundings under the supercritical phase presenting mass densities on the order of magnitude of a liquid. The features of CO₂ are consequently analogous to CH₄, but much more CO₂ can be stored for the same volume.

This particularity of CO₂ compared to CH₄ can be explained by the coordinates of their critical points. The critical point coordinates of CH₄ ($p_{CH_4}^{crit} = 4.5922 \pm 0.002$ MPa, $T_{CH_4}^{crit} = 190.564 \pm 0.012$ K, which were defined by Setzmann and Wagner [31]) are not located in the range of the thermodynamic conditions of the storage because of the critical temperature is too low. Thus, CH₄ enters the supercritical state as the geostatic pressure overcomes the critical pressure, but such a change is not evidenced by discontinuous variations of the thermodynamic parameters. In contrast, the critical point coordinates of CO₂ ($p_{CO_2}^{crit} = 7.3773 \pm 0.0030$ MPa, $T_{CO_2}^{crit} = 304.1282 \pm 0.015$ K which was provided by Span and Wagner [39]) are found within the storage range. This finding implies, that, at a considered temperature lower than $T_{CO_2}^{crit}$, the evolution of the pressure in the cavern must be well controlled to avoid overcoming the gas-saturated pressure, which would trigger an unintended phase transition.

Assuming the presence of a saturated salty-brine, reaching equilibrium also implies the dissolution of the gas into the brine. Calculating the gas solubility into the brine with the Duan-Sun model for both products under the conditions at equilibrium with the surroundings, the evolutions of the maximal gas concentrations of CO₂ and CH₄ are compared in [Figure 5](#). Regardless of the considered depth of storage, the solubility of CO₂ within the brine is much higher than that of CH₄. The change in the slope of the solubility of CO₂ shows its transition from the gas to the liquid phase. This finding tends to confirm the commonly adopted assumption for CH₄, which states that the dissolution of CH₄ into the brine is negligible, but it seems excessive to make such an assumption for CO₂ without any more precise study.

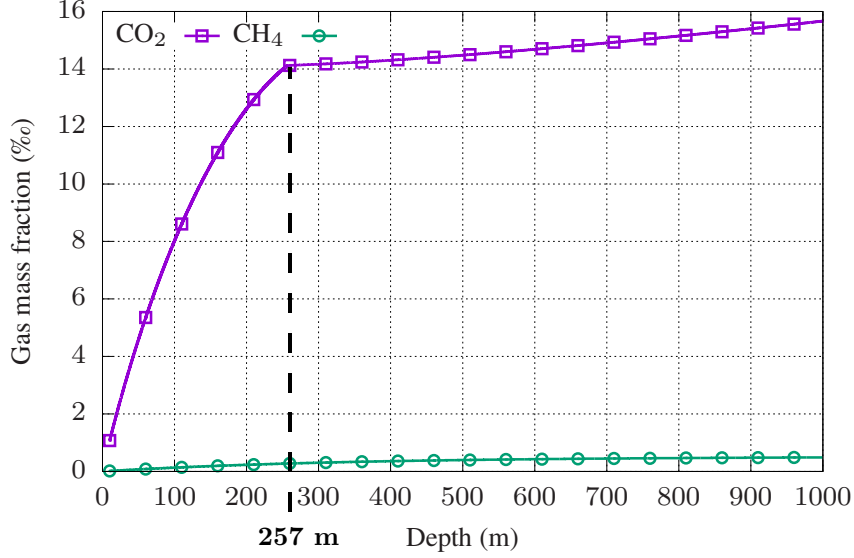


Figure 5: Evolution of the solubilities of CO₂ and CH₄ (expressed in kg of gas/kg of brine) with respect to the depth under geostatic pressure and geothermal temperature

2.4. Thermodynamic behavior comparison in response to real storage operations

This further investigation is achieved by simulating a real storage in salt cavern and observing the storage response to different loading histories. The loss of gas due to dissolution into the brine of the salt cavern is calculated via a posttreatment of the numerical results. To reduce the amount of data, the problem has been reduced as follows: the well is suppressed, the cavern is assumed to be spherical with an initial radius of 20 m and located at an average depth of 800 m under uniform geothermal temperature ($T_\infty = 33^\circ\text{C}$) and geostatic pressure ($p_\infty = 17.6$ MPa). The salt-saturated brine volume is assumed to represent 10% of the whole cavity, while the volume of the insoluble materials is neglected. Finally, as explained in [subsection 2.1](#), the mass transfer from the gas to the brine phase is not taken into account in the calculations. In this illustrative example, the cavern pressure will not be explicitly imposed, but rather the mass flow rate of the gas during injections and withdrawals. Scenarios are built so that the relative mass variation in the cavern $\mathcal{M}(t)/\mathcal{M}(0)$ evolves similarly for both CO₂ and CH₄. These scenarios consist of annual cyclic loadings, composed of an injection period and a withdrawal period and separated by resting periods. As no typical

storage scenario for CO₂ in salt cavern is available, scenarios keeping the average mass of gas per cycle constant are adopted. Many storages of natural gas are managed according to this rule in practice.

In the first scenario, the mass corresponding to 10% of the initial mass of the gas present in the cavity under a pressure of 14 MPa is being withdrawn and then successively injected

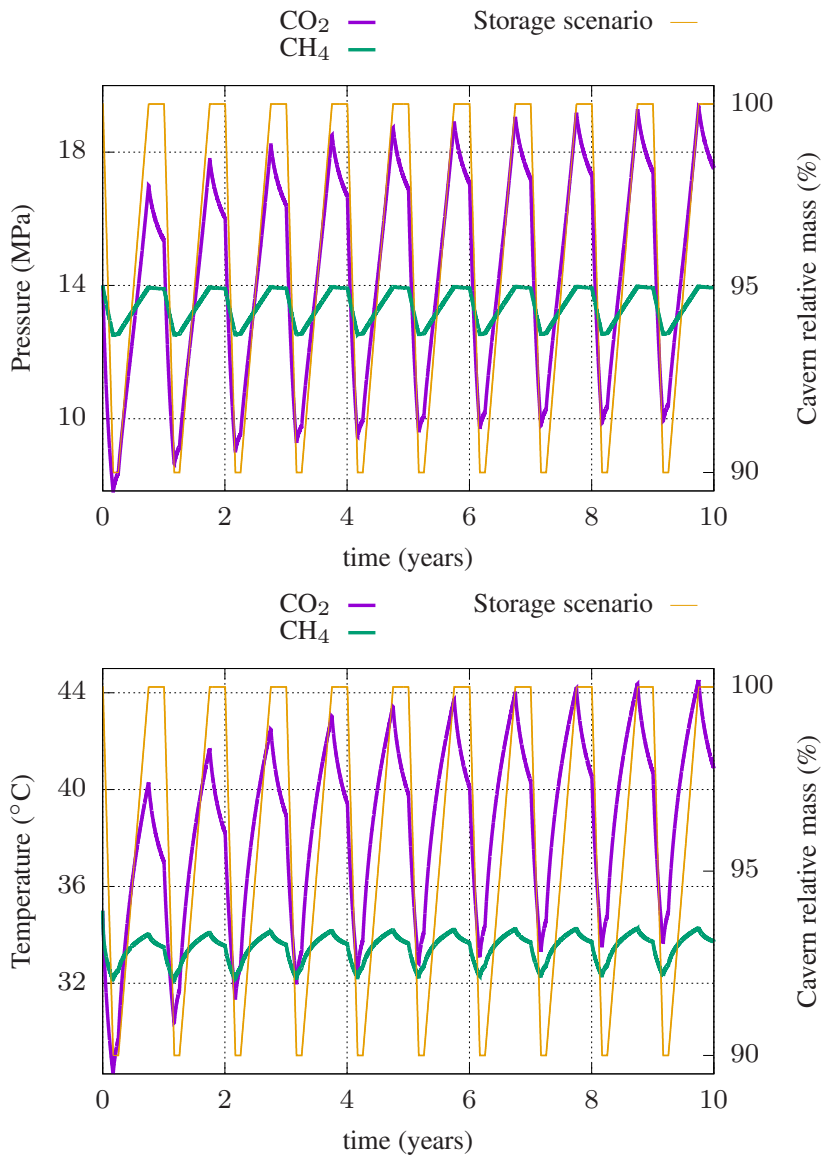


Figure 6: Thermodynamic responses of CO₂ and CH₄ to the first storage scenario, focusing on the storage pressure (top) and temperature (bottom)

and withdrawn. Such a scenario induces different storage behaviors, depending on the considered stored product (see [Figure 6](#)). The average pressure ([Figure 6 top](#)) and temperature ([Figure 6 bottom](#)) per cycle in the storage of CH_4 are stable throughout the considered period, which is not the case for the CO_2 storage, wherein the average pressure and temperature increases rapidly at the beginning before stabilizing. Beyond this global behavior, the main difference between the storages of these two products concerns the amplitudes of the pressure and temperature: CO_2 is submitted to larger variations in temperature and pressure than CH_4 . Consequently, the maximum value of the pressure cycles overcomes the geostatic pressure after 2 cycles. This means that storage following such a scenario is not viable. These high amplitudes are a result of the CO_2 , which is initially stored as a supercritical fluid, becoming liquid instead of gaseous as the temperature decreases below the critical temperature. CO_2 is thus almost incompressible, which implies an important impact on the pressure of any mass density variation. This finding shows that, even if the storage depth is not located in the domain where CO_2 is liquid at equilibrium ([Figure 4](#)), the problem of its thermodynamic state must be carefully handled, as the operations conducted on the storage differ radically when the fluid is liquid or gaseous. In the present study, CO_2 was expected to be stored as a gas, and thus the thermodynamic conditions must never be so that CO_2 is stored as a liquid.

This first scenario tends to indicate that the thermodynamic behavior of CO_2 is not similar to that of CH_4 and cannot be predicted through an analogy with another product stored under the same conditions. Indeed, an acceptable CH_4 storage scenario may be simultaneously unviable for CO_2 . Besides, the cavern capacity which decreases slowly for CH_4 storage due to the creeping behavior of salt rock declines much more over time if CO_2 is stored. Potential problems of storage capacity can be induced in the medium-long term. At last, this scenario can also lead to the forbidden case of CO_2 phase transition; for instance, if 15% of the initial mass of CO_2 is withdrawn, the phase transition phenomenon occurs within the cavity. Thus CO_2 is sometimes stored simultaneously under both liquid and gaseous phases. Because of the features of CO_2 , the storage scenarios must be specifically built and adapted for CO_2 , instead of adopting those used for CH_4 .

A second scenario is considered that assumes an initial pressure of 6 MPa and begins with an injection that introduces an amount of 150% of the initially stored gas in the cavern. As in the first scenario, the maximum temperature per cycle (Figure 7 bottom) increases during the first cycles and stabilizes later. However, compared to the results of the first scenario, the amplitude of the pressure cycles (Figure 7 top) is much more restricted for

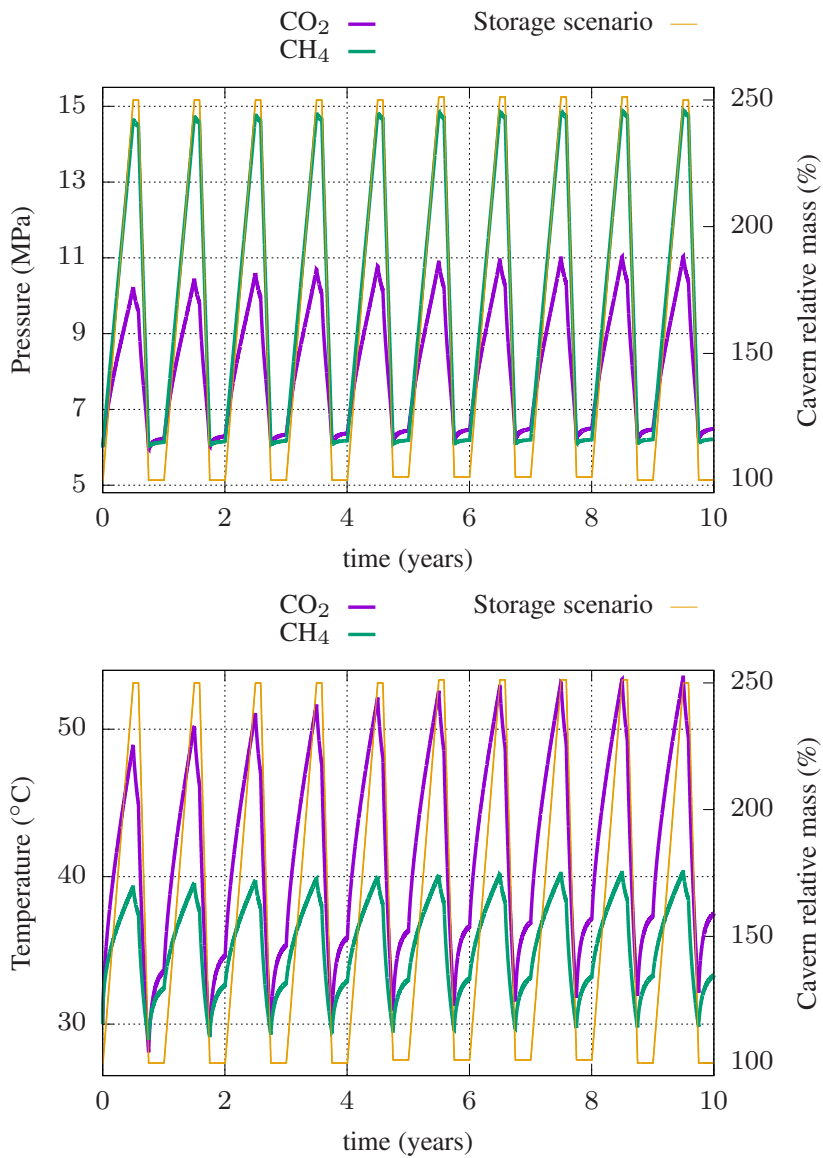


Figure 7: Thermodynamic responses of CO₂ and CH₄ to the second storage scenario, focusing on the storage pressure (top) and temperature (bottom)

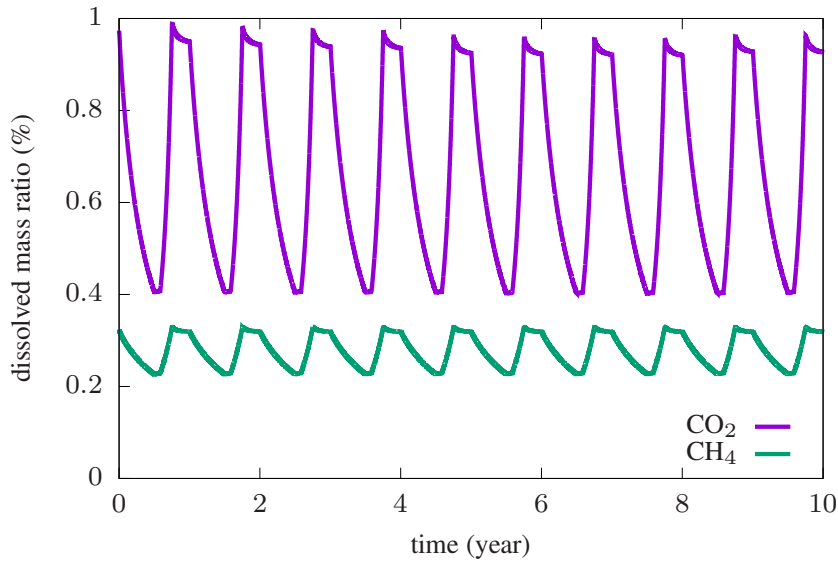


Figure 8: Calculated ratio of the mass of dissolved gas over the total mass of gas stored in the cavity, following the scenario presented in Figure 7 and the Duan-Sun model [33]

CO_2 and larger for CH_4 , which makes such a scenario viable for both products and rather exploitable to estimate the loss of gas from dissolution, as presented in Figure 8.

This figure shows that the importance of gas loss is correlated with the storage history and can represent up to 1% of the total stored mass for CO_2 . The amount of gas loss is higher for CO_2 than for CH_4 , but not as much as expected, according to Figure 5. This finding is attributed to the greater mass density of stored CO_2 compared to that of CH_4 , which provides a higher mass for the same storage volume and partly compensates for the higher mass of dissolved gas.

Two main questions are raised by this figure: why is the CH_4 dissolution in the brine so commonly neglected in practice? Analogously, could the CO_2 interaction with the brine also be neglected? This last question is equivalent to asking if the loss of CO_2 from dissolution are restricted enough not to need to be taken into account in practice, similar to way CH_4 is handled. To answer these questions, experiments aiming to reproduce storage in a salt cavern to study the evolution of the interactions between CO_2/CH_4 and brine must be achieved. These issues will be addressed in the upcoming section.

3. Experimental investigation of the storage behavior of CO₂

The goal of this experiment is to reproduce a storage cavity at a laboratory scale and study the evolution of mass transfer, occurring from the gaseous phase to the liquid phase over time. The final target is to determine the characteristic time of dissolution of CO₂ into the brine, which depends on the conditions of storage and the salinity of the brine, for comparison with the dissolution of CH₄ into the brine. This study is performed to determine whether the time needed to reach the saturation concentration of the gas into the whole brine is long compared to the usual storage periods. This investigation is conducted through the experimental observation of the mass transfer (see [subsection 3.1](#) and [subsection 3.2](#)) and a numerical modeling of the phenomenon (presented in [subsection 3.3](#)) so that the results can be extended to more realistic storage conditions in salt caverns.

The mass transfer is generally characterized by the following parameters: the coefficient of diffusion and the solubility of the gas into the liquid. Both parameters can be experimentally determined through different methods. Among them, methods based on measurements in PVT (pressure-volume-temperature) cells are increasingly important. The goal of such measurement methods is to bring a gaseous and a liquid phase into contact and let a system {liquid + gas} reach its thermodynamic equilibrium naturally while measuring the evolution of an external physical parameter, which can be linked to the mass transfer [40]. This observed parameter can be the pressure in a constant-volume cell (this method is called the Pressure Decay method), the volume of the gaseous phase contained in the cell under a constant pressure (see [41]), or the amount of gas added into the system so that the volume of the cell and the pressure of the gas remains constant (method applied by Haugen and Firoozabadi [42]). The Pressure Decay method is usually applied to measure the absorption of refrigerants [43], the oil and gas recovery in reservoirs [44, 45], the swelling of a liquid phase due to gas dissolution [46], and diffusion coefficients [47]. This method is the most appropriate method for reproducing storage in a salt cavern, because the isochoric PVT cell can play the role of an unalterable cavern at the laboratory scale. Some experiments have already applied the Pressure Decay method to study the mass transfer in several gas-liquid

systems (especially CO₂ and CH₄ in pure water, heavy oil and bitumen; for example Gholami et al. [48], Civan and Rasmussen [49], Upreti and Mehrotra [50], and Unatrakarn et al. [51]), but no study has currently focused on a system {gas - salty brine}. As the solubilities of CO₂ and CH₄ in brine are strongly dependent on the salinity, the whole mass transfer is potentially affected by the presence and concentration of salt, which suggests that the characteristic time of dissolution is also concerned. However, no data about the evolution of the interaction of CO₂ and CH₄ with a NaCl brine over time can confirm this hypothesis. This gap has been bridged in the present work by applying the Pressure Decay method. These tests were performed with three salinities of brine: pure water (salt mass fraction $x_1 = 0\%$), mildly salty brine (salt mass fraction $x_2 = 11 \pm 0.1\%$) and highly salty brine (salt mass fraction $x_3 = 22.5 \pm 0.1\%$) to show the influence of the presence of NaCl on the mass transfer and try to reproduce the salt-saturated brine remaining in caverns. A highly salty brine has been used rather than an NaCl-saturated brine (salt mass fraction of approximately 26%) to avoid the risk of massive crystallization in the tubes and the PVT cell. In addition to the impact of salt on the mass transfer of CO₂ into the brine, the influence of the brine volume in the cell was also studied by performing experiments with 7 different brine volumes, varying in a range of $V_1 = 8$ mL to $V_7 = 85$ mL, in the 96 mL cell volume.

In the presented experiments, a hermetically closed cylindrical cell (internal diameter $d_0 = 4$ cm and height $h_0 = 8$ cm, as shown in the schema in Figure 9) is immersed into a bath that keeps the internal temperature of the cell constant at $T_0 = 40 \pm 0.2^\circ\text{C}$. The pressure in the cell is measured continuously with a pressure tube (calibrated for the pressure range of 1 to 50 bar with an accuracy of ± 6 mbar). Two platinum temperature sensors are placed on the top and on the bottom of the cell to ensure that the temperature within the cell corresponds to T_0 , especially at the beginning of the test. These temperature sensors were calibrated for the temperature range of 5 - 75 °C with an accuracy of $\pm 0.03^\circ\text{C}$. An agitation apparatus that consists of blades and is controlled by an electromagnetic system is added within the cell to accelerate the mass transfer. This agitation device is used to only confirm that the equilibrium between both phases has effectively been reached. At time $t = 0$, gas is introduced into the cell as quickly as possible until the internal pressure reaches

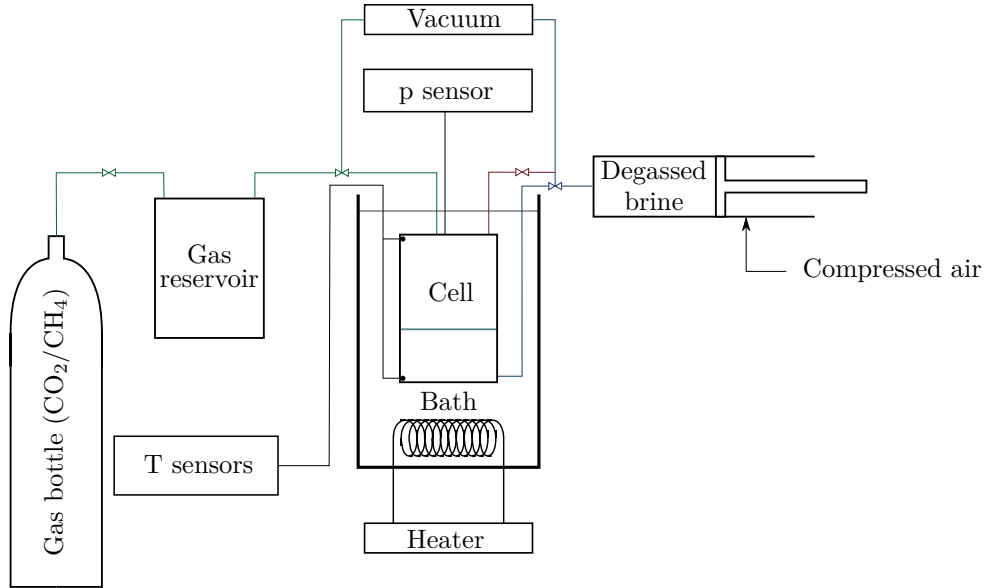


Figure 9: Schema of the experimental apparatus

approximately $P_0 = 10.5$ bar. The cell is then hermetically closed, and the gas pressure is regularly recorded until reaching equilibrium (i.e., when the pressure of the system no longer evolves).

3.1. Experimental behavior comparison of CO₂ and CH₄ stored in the PVT cell

To make the mass transfer and its evolution more obvious, the tests are performed in the PVT cell with a brine volume that is much greater than the volume of gas ($V_{brine} = 80$ mL, which represents about 5 times the volume of gas). These tests have been achieved with pure water and highly salty brine. The behaviors of CO₂ and CH₄ are compared in Figure 10, which confirms that the mass transfer is linked to the pressure drop. This phenomenon is nevertheless much faster and stronger for CO₂, irrespective of the considered brine salinity. In pure water, the CO₂ storage seems to quickly reach its equilibrium (in approximately 4 hours), while the pressure drop at the end of the test for CH₄ is still lower than 0.5 bar at the end of the experiment (its total pressure drop is expected at equilibrium to be greater than 1.5 bar). This phenomenon tends to be slowed in the presence of salt, due to the salting-out effect. The equilibrium with CO₂ is then reached after approximately 20 hours,

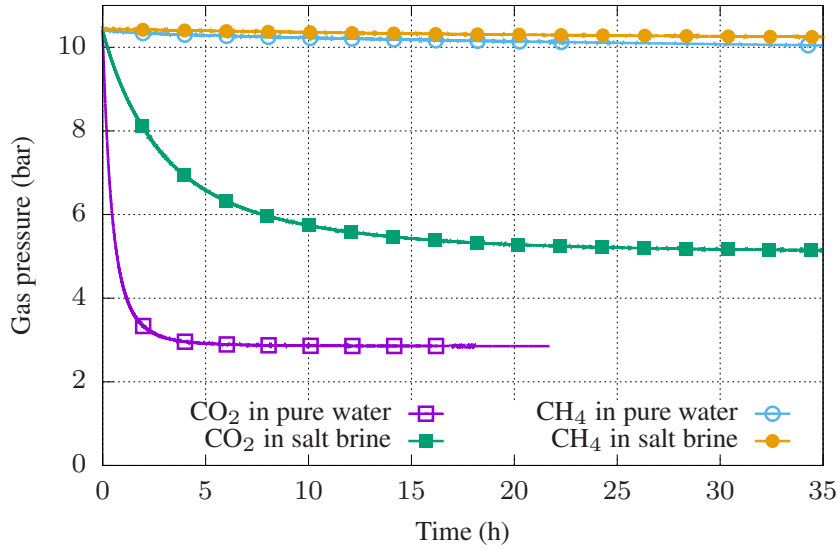


Figure 10: Comparison of the gas pressure evolution with a brine volume $V_6 = 80$ mL for different injected gases (CO_2 or CH_4) and brine salinities ($x_1 = 0\%$ or $x_3 = 22.5\%$)

while the CH_4 pressure drop is almost unnoticeable, thus negligible. These observations conflict with the expectations from the analysis of Figure 8, wherein the mass transfers of CO_2 and CH_4 were expected to be similar despite a lower amplitude of this phenomenon for CH_4 . However, these observations can consistently explain the assumptions adopted in CH_4 storages: if CH_4 effectively dissolves in brine, this phenomenon is too slow to have an impact on the overall storage conditions and to make it noticeable. Rather than the weakness of the dissolution process, the slowness of the dissolution process for CH_4 explains why dissolution does not noticeably impact the thermodynamic conditions during storage periods. In contrast, as the dissolution phenomenon is stronger and faster for CO_2 (as shown in Figure 10), ignoring it potentially induces a noticeable deviation between predictions and metered values, especially concerning the storage pressure.

3.2. Factors impacting the CO_2 pressure drop

A further investigation on the kinetics of the CO_2 interaction with the brine in storage must be achieved to determine whether this interaction is likely to significantly modify the storage conditions and, consequently, whether this interaction has to be taken into account

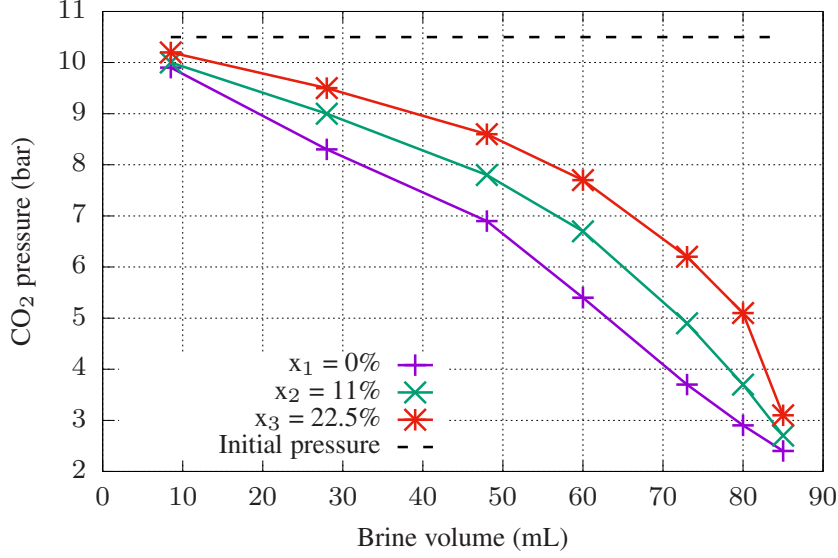


Figure 11: Average measured CO₂ pressure at infinite time (expressed in bar) depending on the brine volume and salinity (expressed in mass fraction of dry NaCl), at the initial pressure $p_0 = 10.5$ bar

in storage modeling. Indeed, if both CO₂ and CH₄ were studied within a PVT cell, in which the brine was in excess (representing 85% of the overall cell volume), in practice, in a salt cavern, the brine volume should not exceed 10% of the total volume. As the mass transfer between the brine and the CH₄ can be considered too slow to be noticed, the current investigation focused on only CO₂ and its interaction with the brine.

As confirmed in Figures 11 and 12, the amplitude of the gas pressure drop from the dissolution at infinite time is influenced by the brine salinity and by the volume of brine remaining within the cavity. During the tests with the brine volume $V_7 = 85$ mL, the equilibrium state is not reached at the end of testing because an insufficient amount of gas was introduced. This is not the case in the other tests. This lack of gas induces other phenomena, which are not in the scope of this article. For this reason, the tests with the brine volume V_7 will not be considered hereafter, and the state at infinite time is assumed to correspond to the equilibrium state. At the equilibrium pressure, the gas concentration in the brine is equal to the gas solubility corresponding to this pressure. During the test, the gas pressure decreases, which reduces the gas solubility but simultaneously increases the

gas concentration in the brine because of the mass transfer. As the salinity of the brine and the volume fraction of the brine phase impact the solubility of the gas and the amount of gas that must be transferred into the brine to reach the saturation concentration, the equilibrium pressure depends on both of these factors.

On the other hand, [Figure 13](#) clearly shows that the response time to reach this equilib-

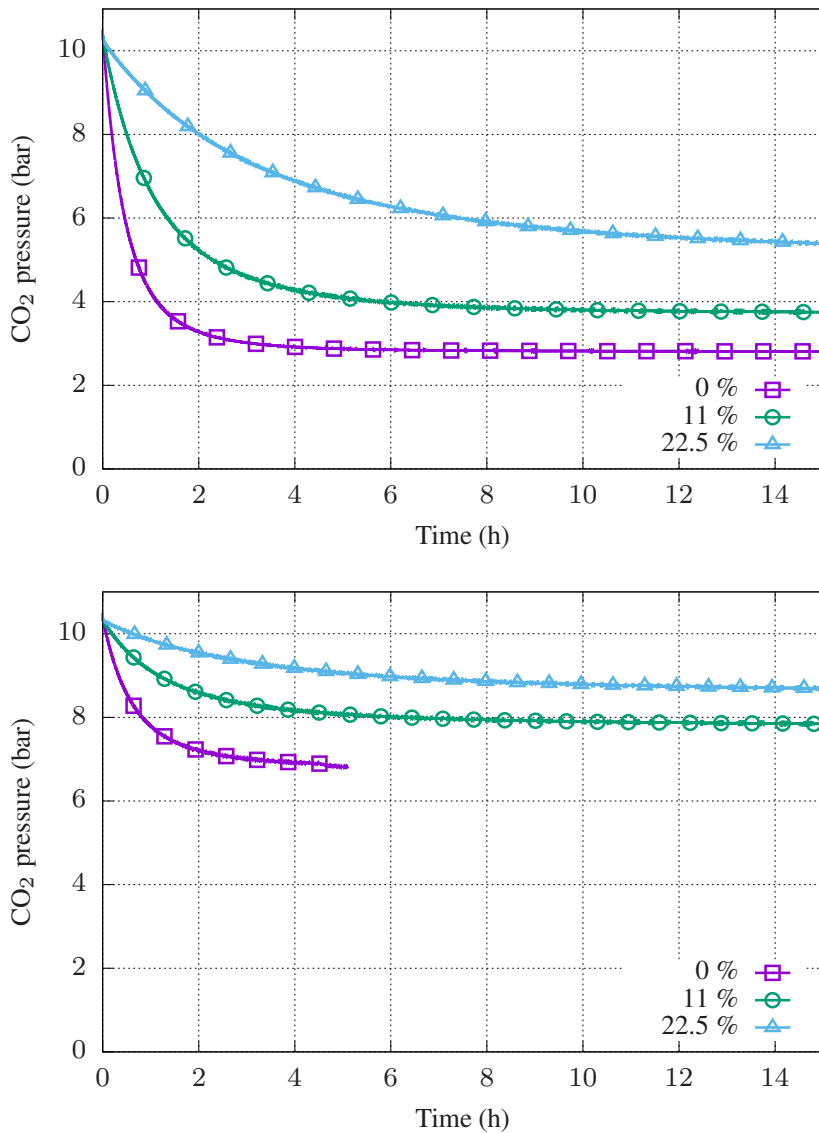


Figure 12: Comparison of the evolution of the gas pressure over time with respect to the brine salinity (x_1 , x_2 and x_3) for brine volumes $V_6 = 80$ mL (top) and $V_3 = 48$ mL (bottom)

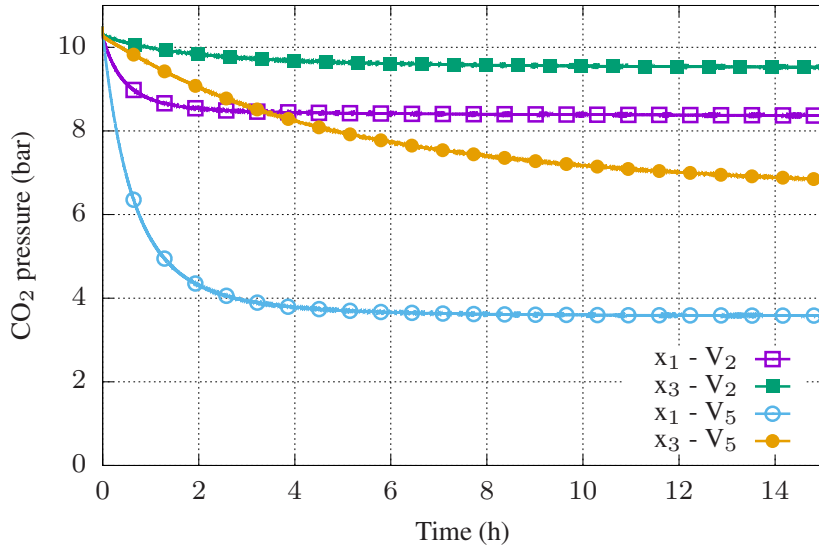


Figure 13: Comparison of the evolution of the gas pressure over time with respect of the salinity of the brine (mass fraction of dry NaCl $x_1 = 0\%$ and $x_3 = 22.5\%$) and the volume of the liquid phase ($V_2 = 28$ mL and $V_5 = 73$ mL)

rium state is also dependent on both of these parameters. Through the salting-out effect, the diffusion of the dissolved gas from the liquid-gas interface to the bottom of the cell slows, increasing the time necessary to reach the equilibrium, in which the gas concentration corresponds to the saturation concentration in the whole liquid phase. The time needed to reach equilibrium is also increased with the total amount of gas that must be solubilized, which is related to the volume fraction of the liquid phase. Thus, the importance of both of these parameters on the rate of the mass transfer must be demonstrated to obtain a reliable estimation of these data under the cavern conditions.

3.3. Comprehensive study of the phenomena linked to the mass transfer

A simplified model that reproduces the evolution of the gas-liquid interaction is proposed. This model aims to reproduce the influences of the brine salinity and the volume ratio of the liquid/gas phases on the mass transfer rate to forecast the duration of the dissolution. This duration is estimated with the characteristic time of dissolution $\tau_{r95\%}$, which corresponds to the time needed for the pressure to decrease up to 95% of the total pressure drop at

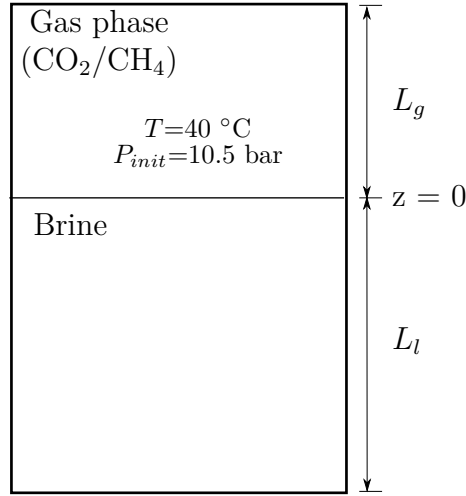


Figure 14: Schema of the modeled PVT cell

equilibrium.

The model focuses on the liquid phase (see [Figure 14](#)) and adopts the following assumptions:

- There is no chemical reaction between the brine and the gas;
- The pressure and the temperature, which is kept constant at $T_0 = 40^\circ\text{C}$ (as confirmed with both temperature sensors placed at the top and bottom of the cell), are uniform within the cell, because of its small size;
- There is no movement of the gas-liquid interface, especially during gas injection, and thus the interfacial area remains constant throughout the test;
- The brine swelling due to the gas dissolution and the water evaporation into the gas phase are neglected. Consequently, the volumes of both phases do not vary over time;
- The saturation concentration is defined through Henry's law formulation $c_g^{sat} = p/H$;
- During the tests, carbon dioxide is considered an ideal gas.

The model is based on a Fickian diffusion law, which can be accurately solved with a one-dimensional formulation. Hence, the mass conservation equation for the dissolved gas in the

liquid phase can be expressed as follows:

$$\frac{\partial c_g}{\partial t} = D \frac{\partial^2 c_g}{\partial z^2} \quad (6)$$

where c_g represents the mass fraction of the dissolved gas in the brine and D is the diffusion coefficient, which is considered to be a constant. Among the different boundary conditions proposed in the literature and summarized by many authors, including for instance Tharanivasan et al. [52] (boundary condition based on the Dirichlet condition [41, 50, 53], on the Neumann condition [54] or on the Robin condition [48, 49, 55]), the nonequilibrium boundary condition at the gas-liquid interface, following Robin condition, has been retained: $-D\partial_z c_g = -K/\rho_l \cdot (c_g^{sat} - c_g^{int})$, where c_g^{int} represents the mass fraction of gas at the gas-liquid interface (at $z = 0$), K is the coefficient of mass transfer, and ρ_l is the mass density of the brine, which is assumed to depend on only the salinity. Such a boundary condition must reliably reproduce the mass transfer evolution, because this boundary condition is supposed to be the closest representation to the physics of mass transfer by including a resistance coefficient ($1/K$) to the phenomenon.

Applying Henry's law and the ideal gas law, the boundary condition, in terms of the evolution of the mass of dissolved gas into the brine, becomes: $\dot{\mathcal{M}}_g(t) = \mathcal{A}K(p(t)/H_{app} - c_g^{int}) \geq 0$, where \mathcal{A} is the CO₂-brine interfacial area, and ρ_g is the gas mass density. The closure of the system is ensured with the equation of the pressure, which describes the gas phase as follows: $\dot{p} = -K_{app}Z_g/L_g(p/H_{app} - c_g^{int})$, where Z_g is a constant resulting from the ideal gas law assumption $p = \rho_g Z_g$, since the temperature remains constant throughout the performed tests, and L_g denotes the gas height ($L_g = V_g/\mathcal{A}$, as shown in Figure 14). Parameters D , H and K are adjusted using the experimental results presented in subsection 3.2. The calibration is achieved in Appendix A.

As presented in Appendix A, the calibration of Henry's factor H provides satisfying results, regarding the literature data. On the other hand, it is more difficult to validate the results of this second step by comparing the calibrated D and H with the data provided in the literature for two main reasons: the first reason concerns the lack of data for the ternary system {H₂O - NaCl - CO₂} because the brine salinity becomes an additional variable of the

Brine salinity	H (MPa/mass fraction)	D (m ² /s)	K (kg/s/m ²)
$x_1 = 0\%$	100	1.4×10^{-7}	0.025
$x_2 = 11\%$	180	9.0×10^{-8}	0.025
$x_3 = 22.5\%$	290	5.0×10^{-8}	0.010

Table 1: Calibration of the model parameters as a function of brine salinity (expressed in mass fraction of dry NaCl)

system thermodynamic data, which complicates their descriptions and reduces the number of data comparable to the calibrated parameters; the second reason concerns the choice of a Fickian model to reproduce the storage behavior. The comparison with the literature data can thus be performed for CO₂ dissolution in only pure water. For such a system, the values of the real diffusion coefficient provided in the literature for this system are approximately 2×10^{-9} m²/s, as measured by Perera et al. [56], Lu et al. [57], Cadogan et al. [58], or Frank et al. [59], which are approximately 2 orders of magnitude lower than the calibrated value and decrease with salinity [56]. As explained in several publications such as Kneafsey and Pruess [60], Farajzadeh et al. [61] and Ennis-King and Paterson [62], Fickian diffusion is not the only phenomenon occurring during CO₂ dissolution into brine or pure water. Other phenomena such as the density-driven natural convection also occur, which reduce the importance of diffusion in the kinetics of the mass transfer and consequently the diffusion coefficient D . For this reason, the calibrated diffusion and mass transfer coefficients, which impact the kinetics of the mass transfer, must be considered as apparent because they result from a calibration of a simple Fickian model and are distinguished from the physical coefficients, which are intrinsic to the observed liquid-gas systems. In the present work, the calibrated diffusion coefficient is consistent with the apparent diffusion coefficients provided in the literature for the system {H₂O - CO₂} (approximately 2×10^{-7} m²/s [45, 63, 64]), which confirms the results of the calibration. However, using a more complex model that integrates all the phenomena occurring during the dissolution and the regimes of diffusion within the brine is unnecessary, as such an integration implies velocity fields in the different phases present within the cavity, which are not taken into account in most of the numerical

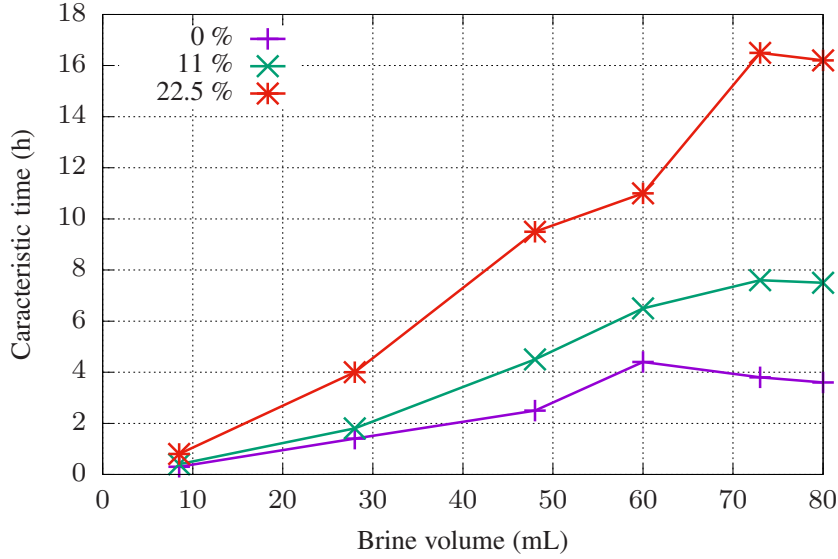


Figure 15: Average characteristic time of dissolution (in h) as a function of the brine volume and salinity (expressed as a mass fraction of dry NaCl)

codes relative to gas storage simulations because of the assumption of the uniformity of the thermodynamic conditions.

The evolution of the characteristic time of dissolution $\tau_{r95\%}$ can be deduced from the calibrated model. The evaluation of the characteristic time of dissolution for every adopted brine volume and salinity during the experiments is presented in Figure 15. It can be easily observed that $\tau_{r95\%}$ is strongly impacted by the volume and salinity of the brine. The salinity tends to slow the diffusion, increasing the characteristic time of dissolution. The volume fraction of the brine phase has a more complex impact on the characteristic time of dissolution: increasing the volume fraction of the brine first induces an increase in the characteristic time until reaching a maximum, and then the characteristic time tends to decrease. This inversion that occurs at the so-called brine volume V_{lim} may be explained by the total mass of gas dissolved within the brine, which increases until a certain brine volume and then decreases, and by the height of the brine phase L_l , which is directly linked to the brine volume. Beyond V_{lim} , the expansion of the mass transfer duration due to the increase in the brine volume is compensated with the smaller amount of gas that must dissolve to

reach the equilibrium, and thus the characteristic time of the mass transfer is reduced. V_{lim} is dependent on the brine salinity because both K and D implied in the diffusion and the temporal evolution of the mass of dissolved gas in brine depend on only the brine salinity. This case is however out of the scope of this article because the volume of the brine in a salt cavern used for gas storage represents too small of a fraction of the whole cavity volume (generally estimated to approximately 10%) compared to the volume fraction at which the inversion phenomenon occurs. In a gas storage context, it can consequently be assumed that the CO_2 characteristic time of dissolution increases with the volume of the brine.

This investigation on the characteristic time of dissolution is important and must be deepened, especially at a cavity scale and under more appropriate storage conditions in terms of pressure and temperature. Indeed, as CO_2 dissolution must be taken into account, the way this interaction will be handled strongly depends on the order of magnitude of its characteristic time. If the characteristic time is large compared to the storage periods, then the CO_2 -brine interaction may be neglected, analogous to the treatment of dissolution for CH_4 ; on the contrary, if the characteristic time is much lower, the interaction may be considered instantaneous: kinetic aspects of the dissolution are ignored and equilibrium between both phases is immediately reached. In the case of a moderate characteristic time, a kinetic model of the dissolution must be added to the global cavity model. In this last case, an accurate model of the storage behavior must be established, as the pressure drop induced by the mass transfer must be well described to avoid confusing this mass transfer-induced pressure drop phenomenon in practice with the consequences of other phenomena, such as the pressure drop caused by gas leakages.

4. Conclusion

Massive reversible carbon dioxide storage is a solution for the potential problem of carbon dioxide supply that can face some energy storage concepts such as the Power-to-Gas process. Salt caverns stand among the most relevant technical solutions to solve this challenge. In this context, this study is the first to address the problems of carbon dioxide temporary storage in such facilities. This study presents the particularities of a storage behavior of

carbon dioxide, compared to the behavior of other already well known products, for which important feedback has been accumulated over decades. The possible technical problems induced by the storage of carbon dioxide are presented as well:

- First, the thermodynamic data of the carbon dioxide critical point belong to the pressure-temperature storage range experienced in salt caverns. Therefore, special attention is required to define beforehand the carbon dioxide thermodynamic state as it is stored and to ensure that no phase transition could occur within the cavity.
- Second, the carbon dioxide-brine interaction potentially affects storage management. Thus, the dissolution of carbon dioxide into brine is more important and kinetically much faster than that in other commonly stored products.

Further modeling and experimental investigations that more precisely evaluate the impact of dissolution on the global storage and the characteristic time of the mass transfer under salt cavern conditions are required. These investigations, which are specific to carbon dioxide, must make more precise quantifications of the amount of gas likely to dissolve, the time needed to reach equilibrium between both phases and the expected pressure drop, whose existence has been revealed. These obstacles and the adaptation of the future storage scenarios of carbon dioxide to the energy demand must be removed to apply the electrolysis-methanation-oxy-fuel solution at an industrial scale.

Acknowledgments

The authors would like to thank Pr. Alain Gaunand (CTP MINES ParisTech), Mr. Alain Valtz (Laboratory of CTP MINES ParisTech) and Pr. Michel Tijani (Géosciences MINES ParisTech), for their contributions to this work. The authors are also thankful towards the ANR project FluidSTORY (n° 7747, ID ANR-15-CE06-0015) for sharing relevant information to this work.

References

- [1] M. Raju, S. K. Khaitan, Modeling and simulation of compressed air storage in caverns: A case study of the Huntorf plant, *Applied Energy* 89 (1) (2012) 474 – 481, ISSN 0306-2619.
- [2] S. Bauer, A. Dahmke, O. Kolditz, Subsurface energy storage: geological storage of renewable energy—capacities, induced effects and implications, *Environmental Earth Sciences* 76 (20) (2017) 695.
- [3] A. Cavallo, Controllable and affordable utility-scale electricity from intermittent wind resources and compressed air energy storage (CAES), *Energy* 32 (2) (2007) 120 – 127, ISSN 0360-5442.
- [4] S. Succar, R. Williams, *Compressed Air Energy Storage: Theory, Resources, And Applications For Wind Power*, Tech. Rep., Princeton Environmental Institute, 2008.
- [5] M. Budt, D. Wolf, R. Span, J. Yan, A review on compressed air energy storage: Basic principles, past milestones and recent developments, *Applied Energy* 170 (2016) 250 – 268.
- [6] M. Lehner, R. Tichler, H. Steinmüller, M. Koppe, *Power-togas: technology and business models*, Springer, 2014.
- [7] M. Götz, J. Lefebvre, F. Mörs, A. M. Koch, F. Graf, S. Bajohr, R. Reimert, T. Kolb, Renewable Power-to-Gas: A technological and economic review, *Renewable Energy* 85 (2016) 1371 – 1390.
- [8] ADEME, Etude portant sur l’hydrogène et la méthanation comme procédé de valorisation de l’électricité excédentaire, URL <http://www.ademe.fr>, 2014.
- [9] M. W. Ajiwibowo, A. Darmawan, M. Aziz, A conceptual chemical looping combustion power system design in a power-to-gas energy storage scenario, *International Journal of Hydrogen Energy* .
- [10] N. Kezibri, C. Bouallou, Conceptual design and modelling of an industrial scale power to gas-oxy-combustion power plant, *International Journal of Hydrogen Energy* 42 (30) (2017) 19411–19419.
- [11] M. Bailera, P. Lisbona, L. M. Romeo, S. Espatolero, Power to Gas–biomass oxycombustion hybrid system: Energy integration and potential applications, *Applied Energy* 167 (2016) 221 – 229.
- [12] M. Bailera, B. Peña, P. Lisbona, L. M. Romeo, Decision-making methodology for managing photovoltaic surplus electricity through Power to Gas: Combined heat and power in urban buildings, *Applied Energy* 228 (2018) 1032 – 1045.
- [13] ANR, Stockage souterrain massif et réversible de vecteurs énergétiques fluides (O₂, CO₂, CH₄), Project No. ANR-15-CE06-0015, URL <http://www.agence-nationale-recherche.fr>, 2016-2020.
- [14] M. Aneke, M. Wang, Energy storage technologies and real life applications – A state of the art review, *Applied Energy* 179 (2016) 350 – 377.
- [15] V. Jülch, Comparison of electricity storage options using levelized cost of storage (LCOS) method, *Applied Energy* 183 (2016) 1594 – 1606.
- [16] M. Procesi, B. Cantucci, M. Buttinelli, G. Armezzani, F. Quattrocchi, E. Boschi, Strategic use of the underground in an energy mix plan: Synergies among CO₂, CH₄ geological storage and geothermal

- energy. Latium Region case study (Central Italy), *Applied Energy* 110 (2013) 104 – 131.
- [17] S. Solomon, M. Carpenter, T. A. Flach, Intermediate storage of carbon dioxide in geological formations: A technical perspective, *International Journal of Greenhouse Gas Control* 2 (4) (2008) 502 – 510, tCCS-4: The 4th Trondheim Conference on CO₂ Capture, Transport and Storage.
- [18] M. D. Aminu, S. A. Nabavi, C. A. Rochelle, V. Manovic, A review of developments in carbon dioxide storage, *Applied Energy* 208 (2017) 1389 – 1419.
- [19] S. Bachu, CO₂ storage in geological media: Role, means, status and barriers to deployment, *Progress in Energy and Combustion Science* 34 (2) (2008) 254–273.
- [20] G. P. D. De Silva, P. G. Ranjith, M. S. A. Perera, Geochemical aspects of CO₂ sequestration in deep saline aquifers: A review, *Fuel* 155 (2015) 128–143.
- [21] N. Spycher, K. Pruess, A Phase-Partitioning Model for CO₂–Brine Mixtures at Elevated Temperatures and Pressures: Application to CO₂-Enhanced Geothermal Systems, *Transport in Porous Media* 82 (1) (2010) 173–196.
- [22] P. Ahmadi, A. Chapoy, CO₂ solubility in formation water under sequestration conditions, *Fluid Phase Equilibria* 463 (2018) 80 – 90.
- [23] L. Tomić, V. Karović Maričić, D. Danilović, M. Crnogorac, Criteria for CO₂ storage in geological formations, *Podzemni radovi* (32) (2018) 61–74.
- [24] A. Rouabhi, G. Hévin, A. Soubeyran, P. Labaune, F. Louvet, A multiphase multicomponent modeling approach of underground salt cavern storage, *Geomechanics for Energy and the Environment* 12 (2017) 21 – 35.
- [25] A. Bağcı, E. Ozturk, Performance prediction of underground gas storage in salt caverns, *Energy Sources, Part B: Economics, Planning and Policy* 2 (2) (2007) 155–165.
- [26] K. Serbin, J. Ślizowski, K. Urbańczyk, S. Nagy, The influence of thermodynamic effects on gas storage cavern convergence, *International Journal of Rock Mechanics and Mining Sciences* 79 (2015) 166–171.
- [27] K. Khaledi, E. Mahmoudi, M. Datcheva, T. Schanz, Analysis of compressed air storage caverns in rock salt considering thermo-mechanical cyclic loading, *Environmental Earth Sciences* 75 (15) (2016) 1149.
- [28] S.-W. Zhou, C.-C. Xia, H.-B. Zhao, S.-H. Mei, Y. Zhou, Numerical simulation for the coupled thermo-mechanical performance of a lined rock cavern for underground compressed air energy storage, *Journal of Geophysics and Engineering* 14 (6) (2017) 1382–1398.
- [29] N. Böttcher, U.-J. Görke, O. Kolditz, T. Nagel, Thermo-mechanical investigation of salt caverns for short-term hydrogen storage, *Environmental Earth Sciences* 76 (3) (2017) 98.
- [30] P. Labaune, A. Rouabhi, Dilatancy and tensile criteria for salt cavern design in the context of cyclic loading for energy storage, *Journal of Natural Gas Science and Engineering* 62 (2019) 314–329.
- [31] U. Setzmann, W. Wagner, A New Equation of State and Tables of Thermodynamic Properties for

- Methane Covering the Range from the Melting Line to 625 K at Pressures up to 100 MPa, *Journal of Physical and Chemical Reference Data* 20 (6) (1991) 1061–1155.
- [32] O. Kunz, W. Wagner, The GERG-2008 Wide-Range Equation of State for Natural Gases and Other Mixtures: An Expansion of GERG-2004, *Journal of Chemical & Engineering Data* 57 (11) (2012) 3032–3091.
- [33] Z. Duan, R. Sun, An improved model calculating CO₂ solubility in pure water and aqueous NaCl solutions from 273 to 533 K and from 0 to 2000 bar, *Chemical Geology* 193 (3–4) (2003) 257–271.
- [34] Z. Duan, S. Mao, A thermodynamic model for calculating methane solubility, density and gas phase composition of methane-bearing aqueous fluids from 273 to 523K and from 1 to 2000bar, *Geochimica et Cosmochimica Acta* 70 (13) (2006) 3369 – 3386.
- [35] N. N. Akinfiev, L. W. Diamond, Thermodynamic model of aqueous CO₂–H₂O–NaCl solutions from -22 to 100 °C and from 0.1 to 100 MPa, *Fluid Phase Equilibria* 295 (1) (2010) 104–124.
- [36] S. Mao, D. Zhang, Y. Li, N. Liu, An improved model for calculating CO₂ solubility in aqueous NaCl solutions and the application to CO₂–H₂O–NaCl fluid inclusions, *Chemical Geology* 347 (2013) 43 – 58.
- [37] Z. Wang, M. J. Small, A. K. Karamalidis, Multimodel Predictive System for Carbon Dioxide Solubility in Saline Formation Waters, *Environmental Science & Technology* 47 (3) (2013) 1407–1415.
- [38] H. Zhao, M. V. Fedkin, R. M. Dilmore, S. N. Lvov, Carbon dioxide solubility in aqueous solutions of sodium chloride at geological conditions: Experimental results at 323.15, 373.15, and 423.15K and 150bar and modeling up to 573.15K and 2000bar, *Geochimica et Cosmochimica Acta* 149 (2015) 165 – 189.
- [39] R. Span, W. Wagner, A New Equation of State for Carbon Dioxide Covering the Fluid Region from the Triple-Point Temperature to 1100 K at Pressures up to 800 MPa, *Journal of Physical and Chemical Reference Data* 25 (6) (1996) 1509–1596.
- [40] N. Policarpo, P. Ribeiro, EXPERIMENTAL MEASUREMENT OF GAS-LIQUID DIFFUSIVITY, *Brazilian Journal of Petroleum and Gas* 5 (3) (2011) 171–188.
- [41] S. R. Etminan, B. B. Maini, Z. Chen, H. Hassanzadeh, Constant-Pressure Technique for Gas Diffusivity and Solubility Measurements in Heavy Oil and Bitumen, *Energy & Fuels* 24 (1) (2010) 533–549.
- [42] K. B. Haugen, A. Firoozabadi, Mixing of two binary nonequilibrium phases in one dimension, *AIChE Journal* 55 (8) (2009) 1930–1936.
- [43] A. Yokozeki, Time-dependent behavior of gas absorption in lubricant oil, *International Journal of Refrigeration* 25 (6) (2002) 695–704.
- [44] A. K. Tharanivasan, C. Yang, Y. Gu, Measurements of Molecular Diffusion Coefficients of Carbon Dioxide, Methane, and Propane in Heavy Oil under Reservoir Conditions, *Energy & Fuels* 20 (6)

- (2006) 2509–2517.
- [45] R. Farajzadeh, P. L. J. Zitha, J. Bruining, Enhanced Mass Transfer of CO₂ into Water: Experiment and Modeling, *Industrial & Engineering Chemistry Research* 48 (13) (2009) 6423 – 6431.
- [46] M. R. Riazi, A new method for experimental measurement of diffusion coefficients in reservoir fluids, *Journal of Petroleum Science and Engineering* 14 (3) (1996) 235–250.
- [47] E. Behzadfar, S. G. Hatzikiriakos, Diffusivity of CO₂ in Bitumen: Pressure–Decay Measurements Coupled with Rheometry, *Energy & Fuels* 28 (2) (2014) 1304–1311.
- [48] Y. Gholami, R. Azin, R. Fatehi, S. Osfouri, A. Bahadori, Prediction of carbon dioxide dissolution in bulk water under isothermal pressure decay at different boundary conditions, *Journal of Molecular Liquids* 202 (2015) 23–33.
- [49] F. Civan, M. L. Rasmussen, Accurate Measurement of Gas Diffusivity in Oil and Brine Under Reservoir Conditions, in: *SPE Production and Operations Symposium*, Society of Petroleum Engineers, 2001.
- [50] S. R. Upreti, A. K. Mehrotra, Experimental Measurement of Gas Diffusivity in Bitumen: Results for Carbon Dioxide, *Industrial & Engineering Chemistry Research* 39 (4) (2000) 1080–1087.
- [51] D. Unatrakarn, K. Asghari, J. Condor, Experimental studies of CO₂ and CH₄ diffusion coefficient in bulk oil and porous media, *Energy Procedia* 4 (2011) 2170–2177.
- [52] A. K. Tharanivasan, C. Yang, Y. Gu, Comparison of three different interface mass transfer models used in the experimental measurement of solvent diffusivity in heavy oil, *Journal of Petroleum Science and Engineering* 44 (3) (2004) 269–282.
- [53] Y. P. Zhang, C. L. Hyndman, B. B. Maini, Measurement of gas diffusivity in heavy oils, *Journal of Petroleum Science and Engineering* 25 (1) (2000) 37–47.
- [54] H. Sheikha, M. Pooladi-Darvish, A. K. Mehrotra, Development of Graphical Methods for Estimating the Diffusivity Coefficient of Gases in Bitumen from Pressure-Decay Data, *Energy & Fuels* 19 (5) (2005) 2041–2049.
- [55] S. R. Etminan, M. Pooladi-Darvish, B. B. Maini, Z. J. Chen, Mass Diffusion Parameters in Presence of Interface Resistance in Gas-Bitumen Systems, in: *Canadian Unconventional Resources and International Petroleum Conference*, Society of Petroleum Engineers, 2010.
- [56] P. N. Perera, H. Deng, P. J. Schuck, B. Gilbert, Diffusivity of Carbon Dioxide in Aqueous Solutions under Geologic Carbon Sequestration Conditions, *The Journal of Physical Chemistry B* 122 (16) (2018) 4566–4572.
- [57] W. Lu, H. Guo, I. Chou, R. Burruss, L. Li, Determination of diffusion coefficients of carbon dioxide in water between 268 and 473K in a high-pressure capillary optical cell with in situ Raman spectroscopic measurements, *Geochimica et Cosmochimica Acta* 115 (2013) 183 – 204, ISSN 0016-7037.
- [58] S. P. Cadogan, G. C. Maitland, J. P. M. Trusler, Diffusion Coefficients of CO₂ and N₂ in Water at

- Temperatures between 298.15 K and 423.15 K at Pressures up to 45 MPa, *Journal of Chemical & Engineering Data* 59 (2) (2014) 519–525.
- [59] M. J. W. Frank, J. A. M. Kuipers, W. P. M. van Swaaij, Diffusion Coefficients and Viscosities of CO₂ + H₂O, CO₂ + CH₃OH, NH₃ + H₂O, and NH₃ + CH₃OH Liquid Mixtures, *Journal of Chemical & Engineering Data* 41 (2) (1996) 297–302, ISSN 0021-9568.
- [60] T. J. Kneafsey, K. Pruess, Laboratory Flow Experiments for Visualizing Carbon Dioxide-Induced, Density-Driven Brine Convection, *Transport in Porous Media* 82 (1) (2010) 123–139.
- [61] R. Farajzadeh, P. Ranganathan, P. Zitha, J. Bruining, The effect of heterogeneity on the character of density-driven natural convection of CO₂ overlying a brine layer, *Advances in Water Resources* 34 (3) (2011) 327 – 339.
- [62] J. P. Ennis-King, L. Paterson, Role of Convective Mixing in the Long-Term Storage of Carbon Dioxide in Deep Saline Formations, *SPE Journal* 10 (03) (2005) 349–356.
- [63] O. Tveteraas, A Study of Pressure Decay in a Closed CO₂-Water System, Master’s thesis, University of Stavanger (NOR), 2011.
- [64] C. Yang, Y. Gu, Accelerated Mass Transfer of CO₂ in Reservoir Brine Due to Density-Driven Natural Convection at High Pressures and Elevated Temperatures, *Industrial & Engineering Chemistry Research* 45 (8) (2006) 2430–2436.
- [65] J. J. Carroll, J. D. Slupsky, A. E. Mather, The solubility of carbon dioxide in water at low pressure, *Journal of Physical and Chemical Reference Data* 20 (6) (1991) 1201–1209.

Appendix A. Calibration of the dissolution parameters

The calibration is conducted in two steps: the first step, which concerns only the equilibrium state of the system, analytically solves the mathematical model, while the second step, which focuses on the transient period, is solved with the finite element method. The adjustment of the parameters is summarized in [Table 1](#). The salting-out effect can be noticed on the evolution of the parameters with respect to the brine salinity: the solubility (parameter H) and coefficients K and D decrease as expected. The presence of NaCl tends to increase the resistance to the mass transfer and slow the diffusion of the CO₂ into the brine.

The analytical expression of the gas concentration at equilibrium c_g^{sat*} is as follows:

$$c_g^{sat*} = \lim_{t \rightarrow +\infty} c_g(t, z) = \lim_{t \rightarrow +\infty} c_g(t) = \frac{p_0}{H + Z_g \rho_l R_v} \quad (\text{A.1})$$

where p_0 is the initial gas pressure ($p_0 = p(t = 0) = 10.5$ bar) and R_v corresponds to the liquid/gas phase volume ratio ($R_v = V_l/V_g = L_l/L_g$). As expected, Henry's factor H is the only parameter implied in the long-term evolution of the mass transfer because it is the single parameter to calibrate when dealing with the saturation and the equilibrium. The results

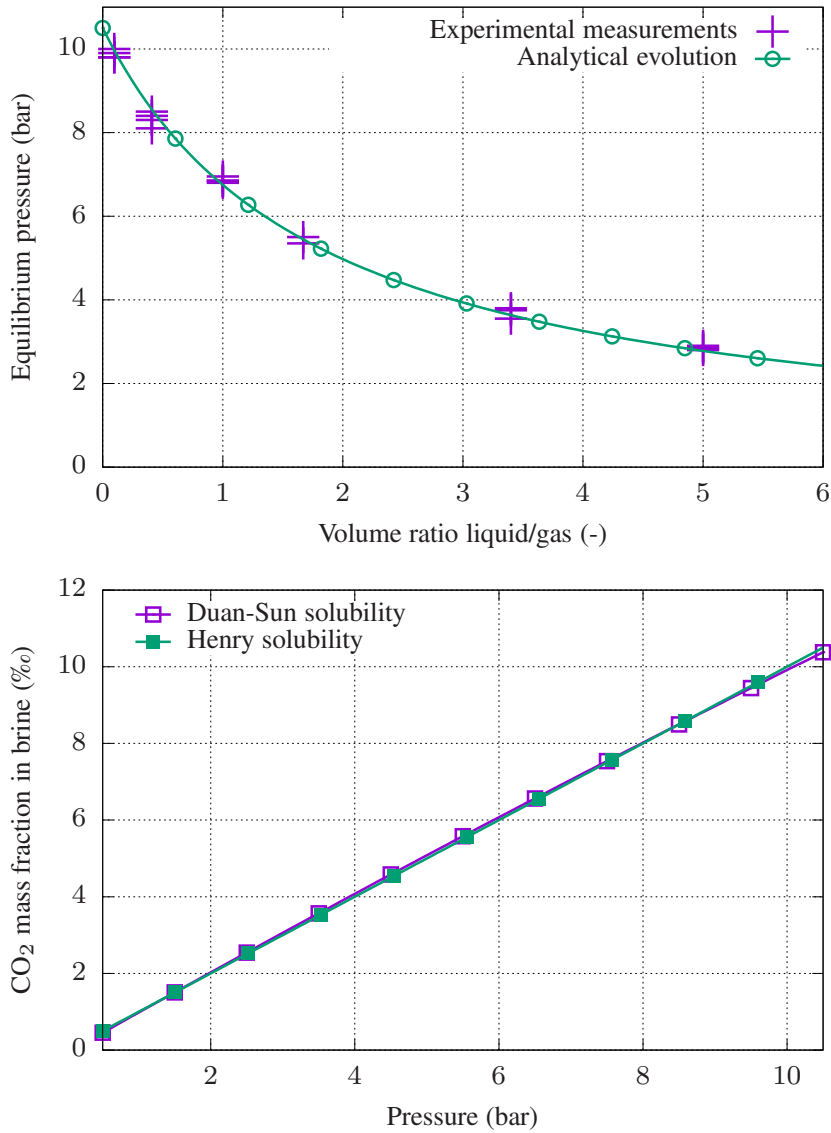


Figure A.16: Calibration results of the Henry's factor H for pure water ($H = 100$ MPa/mass fraction) through the evolution of the equilibrium pressure with respect the liquid/gas volumes ratio (top), and verification of the solubility calculated from the calibrated H with the literature data (bottom)

of the comparison between the analytical gas concentration c_g^{sat*} , which is obtained with the calibrated H , and the values of the experimental gas concentration, which are calculated from the overall measured pressure drop, are shown in Figures A.16 and A.17 (top). To confirm the calibrated value of Henry's factor, the evolution of the CO₂ concentration at saturation with

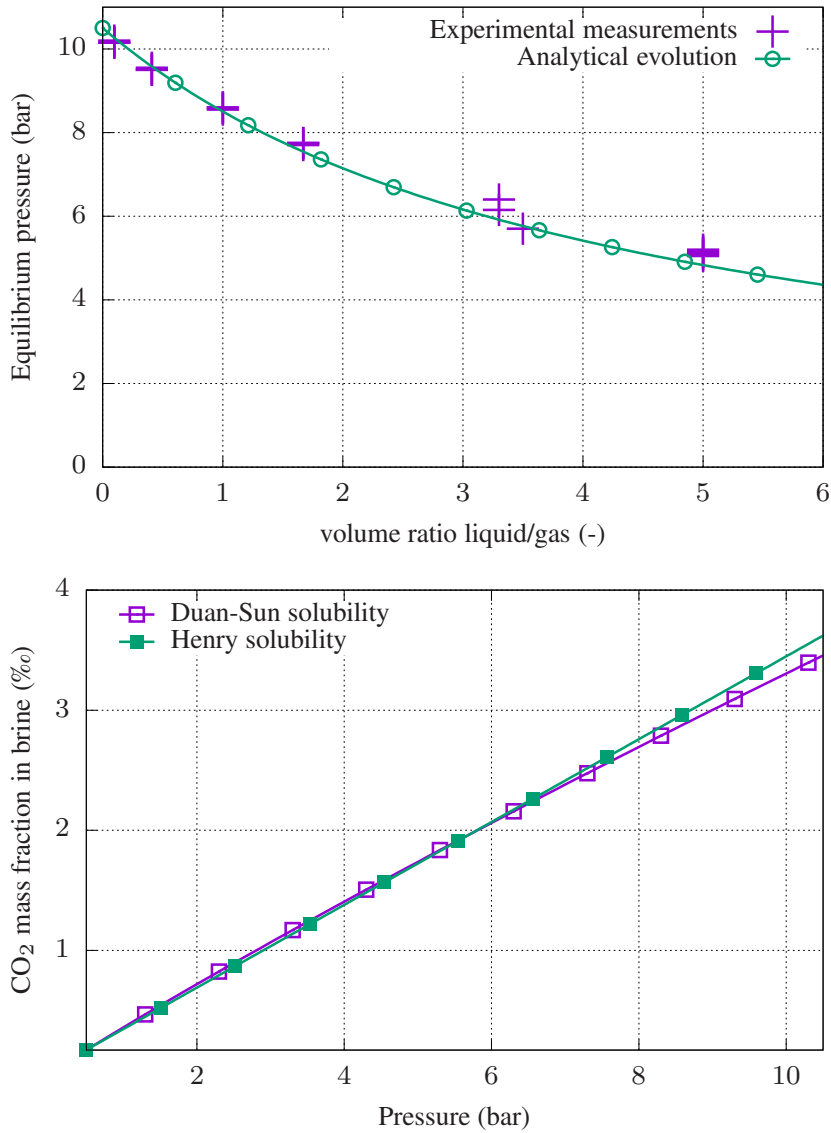


Figure A.17: Calibration results of the Henry's factor H for the highly salty brine ($H = 290$ MPa/mass fraction) through the evolution of the equilibrium pressure with respect to the liquid/gas volumes ratio (top), and verification of the solubility calculated from the calibrated H with the literature data (bottom)

respect to the pressure following Henry’s law is compared to the solubility data according to the Duan-Sun model [33] (see bottom of Figures A.16 and A.17). These comparisons show good agreements between the experimentally measured values, theoretically calculated values and collected data and thus confirm the performed calibration. Indeed, the calibrated parameter H can hardly be compared to the existing values from correlations provided in the literature because no linear relation links the adopted units to those adopted in this study (for example, the correlation proposed in the work of Carroll et al. [65] gives a value of 230 MPa/mol fraction).

Both other parameters D and K , which are numerically calibrated in the transient state, impact the system time response and the initial variation rate of concentration respectively, as shown in [55]. The higher the mass transfer coefficient K is, the quicker the CO_2 concentration increases at the beginning because the concentration at saturation at the interface is reached earlier. The higher the diffusion coefficient D is, the earlier the equilibrium is attained because the gas at the interface diffuses more quickly through the liquid phase, inducing an important mass transfer to maintain the equilibrium at the interface. Simulations

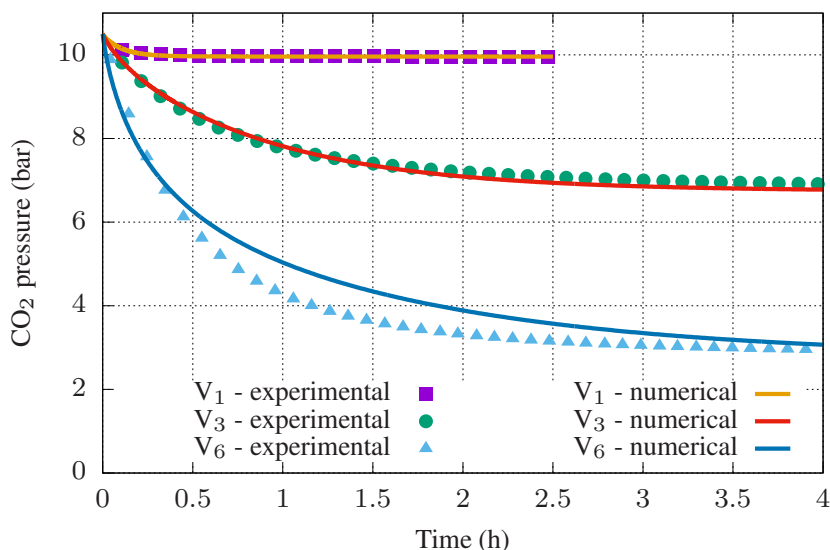


Figure A.18: Comparison of the experimentally measured and numerically computed gas pressure evolution over time in pure water for different brine volumes ($V_1 = 8.5$ mL, $V_3 = 48$ mL and $V_6 = 80$ mL)

of the experiments using the calibrated parameters are presented in Figures A.18 and A.19. The experimental results can be more or less well reproduced with this model, irrespective of the volume of the brine remaining in the PVT cell, which validates the hypothesis of the single dependence of the parameters D and K on the brine salinity.

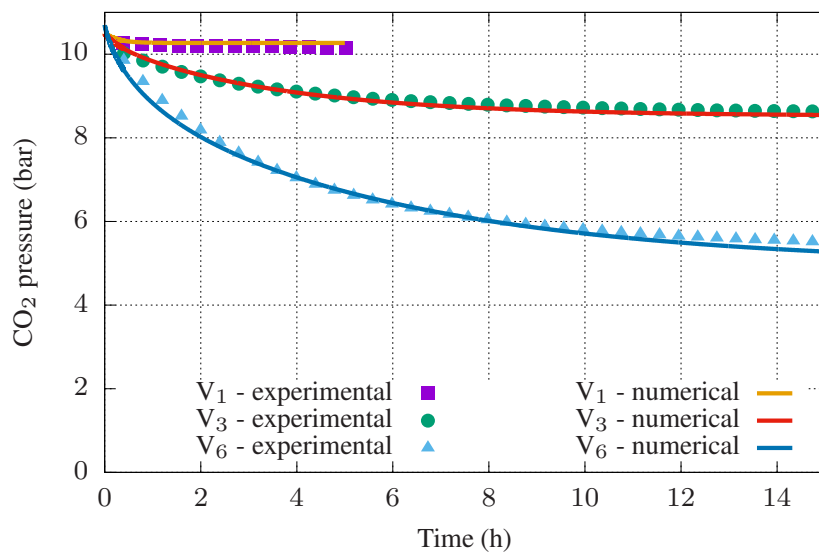


Figure A.19: Comparison of the experimentally measured and numerically computed gas pressure evolution over time in the highly salty brine for different brine volumes ($V_1 = 8.5$ mL, $V_3 = 48$ mL and $V_6 = 80$ mL)